Point-Focusing of Shear-Horizontal Wave Using Fan-Shaped Periodic Permanent Magnet Focusing Coils EMAT for Plate Inspection

Hongyu Sun, Shen Wang, Songling Huang, Senior Member, IEEE, Qing Wang, Senior Member, IEEE, and Wei Zhao

***Abstract*—Ultrasonic guided wave testing method is very effective in safety monitoring of complex structures, such as large-scale tank floor and industrial metal plate. The fundamental shear horizontal (SH) wave mode with the Lorentz force mechanism has the advantage that the propagation velocity does not change with the frequency. However, it is hard to recognize the dispersed ultrasonic signal accurately due to the bidirectional propagation characteristics of the SH guided wave. Therefore, a new transducer structure with a fan-shaped periodic permanent magnet (PPM) and centripetal conductor has been designed to achieve guided wave focusing and signal enhancement. Compared with the traditional transducers, the new-designed transducer has been proved to be more effective in energy focusing on the simulation and experimental verification. For the new structure of the transducer, the aperture angle, focusing radius, and coil rotation angle are studied in detail in this paper. The results show that, as the aperture angle and the coil rotation angle decrease, the signal intensity becomes higher at the focusing position. Moreover, as the focal radius increases, the amplitude of the ultrasonic signals on the focusing side and the divergent side will decrease, while the difference between the two sides will increase exponentially. In the defect detection in this paper, the reflected signal intensity of the new-designed fan-shaped PPM focusing coils electromagnetic acoustic transducer (EMAT) is approximately two times that of the traditional parallel PPM parallel coils EMAT. Therefore, the newly designed EMAT is of great significance for the signal enhancement.**

***Index Terms*—SH guided wave, point focusing, periodic permanent magnet, aperture angle, focal radius, rotation angle.**

I. Introduction

At present, an ultrasonic testing method with the advantages of strong penetrating ability, high accuracy, and high sensitivity is commonly utilized in the defect detection for aluminum plates [1]–[4]. When the ultrasonic bulk wave propagates in a waveguide such as a metal plate, an ultrasonic guided wave is generated and propagates along the extending direction of the waveguide [5], [6]. Ultrasonic guided wave testing method based on the piezoelectric ultrasonic transducer is commonly used to detect defects of the metal plates, and the ultrasonic waves could be excited by the piezoelectric ultrasonic transducers and the couplant material [7], [8]. Since such a transducer requires the couplant to transmit the vibration, it is not suitable for the detection in extreme environments such as high temperature and pressure [9]. Electromagnetic acoustic transducers (EMATs) mainly exchange energy by the coupling of the electromagnetic fields, so the couplant is not required, as with a piezoelectric transducer [10]–[15]. As one of the commonly used guided wave modes in the detection of metal plates, the Shear Horizontally (SH) polarized guided wave does not produce out-of-plane displacement because of its particular polarization mode. Therefore, it is not affected by the carrier medium on the plate surface, such as the measuring instruments and industrial equipment [16], [17]. The fundamental Shear Horizontally (SH0) guided wave mode has the advantages of small signal strength attenuation and no modal conversion during the wave propagation [18]. Therefore, the use of a fundamental mode and non-dispersive SH0 mode guided wave is beneficial to improving the intensity of the detection signal and the efficiency and accuracy of the detection process [19].

Two basic methods to excite the SH guided wave in the metal plate by using the EMAT can be summarized as follows. One is based on the principle of magnetostriction; the other is the Lorentz force. In non-ferromagnetic materials such as aluminum, only the Lorentz force mechanism exists. As for the ferromagnetic materials, these two mechanisms exist simultaneously while the magnetostriction has been proved to be dominant [20]. Since the direction of the applied magnetic field coincides with the current direction of the coils, and they are both parallel to the plate surface. Therefore, the Lorentz forces are not generated inside the steel plate where the dynamic and static magnetic fields exist. Due to the magnetostriction, the surface of the plate generates a reciprocating vibration, and the SH wave propagates along the vertical direction of the vibration direction. As for the EMAT based on the Lorentz force mechanism, periodic permanent magnets (PPM) and parallel coils are utilized to excite SH guided waves in the metal plate; and it can be used for both ferromagnetic and non-ferromagnetic materials. This kind of EMAT has the advantages of small reflection, beam steering, and good environmental adaptability.

The SH guided wave EMAT based on the Lorentz force mechanism commonly has a symmetrical structure so that the generated SH guided wave propagates bidirectionally along both sides of the specimen on the plate [21]. The bidirectional propagation not only leads to the superposition, interference,

and attenuation of the waves, which makes it hard to recognize the signal in the noise but also disperses the energy of the signal with a low signal-to-noise ratio [22]. In 1990, Thompson [23] found that the angle of SH emission can be controlled by exciting the unidirectional SH guided wave using the PPM EMAT based on the principle of structural interference and applying current pulses of different excitation frequencies. However, the application of the wideband signal for changing the emission angle affects the strength of the obtained signal, so small defects might be missed when this method is utilized. In 2016, Zhang et al. [24] proposed a direction-controllable SH wave EMAT based on the principle of magnetostriction for the steel plate. A mechanical structure that can be rotated with the coils' selectivity was proposed by Zhang to control the direction in which the SH guided wave is excited. However, the structure of the above EMATs can only select the propagation direction of the SH wave, but it cannot improve the signal strength of the SH guided wave. In 2017, Song and Qiu [25] focused the beam of the SH guided waves on one side by using two EMAT coils and rotated the traditional parallel coils by an angle. This specific transducer structure can focus and increase the signal strength unidirectionally to a certain extent. However, this method uses more than one EMATs, which may generate additional reflection and refraction of the SH waves and requires a certain mechanical structure for the direction adjustment. It can be seen from the above studies that there are still many problems in the detection of SH guided waves on the plate, and the problem of the low energy conversion efficiency of EMAT needs to be solved urgently such as in the defect detection of the industrial tank floor. Although focusing methods for SH guided waves have been investigated before, these methods still need to be improved.

In this paper, Section II introduces the modeling process of this study. Section III presents the characteristics of the newly designed EMAT through simulation, and Section IV reports and analyzes the simulation and experimental measurement results of the proposed EMAT. In the study, a new configuration structure of a fan-shaped PPM focusing coils EMAT is proposed for inspecting the aluminum plates, which can focus the SH wave at one point and increase the signal intensity and reduce the amplitude of the wave on the divergent side. A three-dimensional model is built using COMSOL software with electromagnetic and solid mechanics modes. The distributions of the displacement field at three particular moments are shown and the calculations of the new EMAT and the traditional parallel EMAT are compared. The effects of the aperture angle and the focal radius are investigated through numerical simulation and experimental validation. The effect of different rotation angles of a single coil on the normalized displacement amplitude of the focal point position is also discussed in the paper. The results show that the new-designed EMAT has great advantages in signal focusing and are shown effective in the defect detection for aluminum plates.

II. MODEL DESCRIPTION

In order to characterize the new-designed point-focusing EMAT with PPM, geometric and physical models are utilized to describe the configuration of the structure in detail. The simulation is implemented using Finite Element Method (FEM), and the numerical algorithm of the calculation is also introduced. Moreover, the same model described in different methods is described in the following sections.

A. Geometric Model

To introduce the structure of the new transducer clearly, its geometric diagram is shown in Fig. 1. Since the effects of the physical variables (such as the aperture angle θ, focal radius r and rotation angle ϕ) on the new transducer need to be discussed, no definite values are specified for these parameters. As shown in the figure, the new transducer consists of a fan-shaped periodic permanent magnet with seven centripetal coils while the center of the coil is defined as the focal point. The propagation direction of the SH guided wave excited by the Lorentz force is pre-determined as it propagates bidirectionally along the surface of the aluminum plate and perpendicular to the vibration direction of the shear waves. Therefore, the focal point of the seven coils in Fig. 1 could also be regarded as the focusing position of the ultrasonic waves. The top view of the transducer's structure is also shown in the figure while the aperture angle θ refers to that between the first coil and the last coil. The focal radius marked in the figure refers to the radius of the concentric coils.

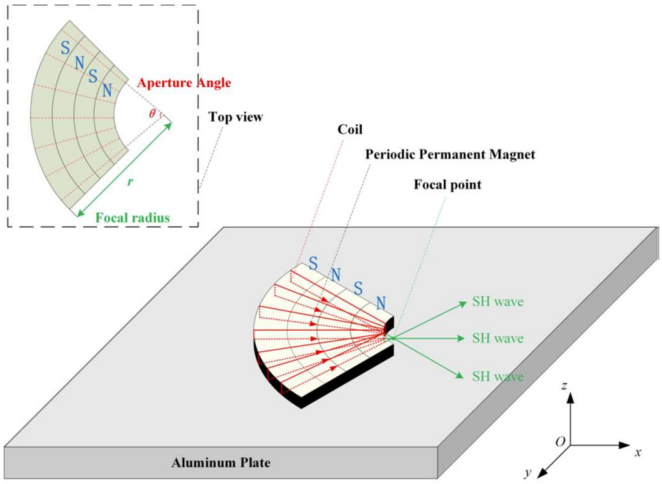

Fig.1 Schematic diagram of the new designed SH guided wave focusing electromagnetic acoustic transducer

B. Physical Model

Ultrasonic guided wave testing method based on Lorentz force mechanism is widely used as the most important tool for nondestructive testing of an aluminum plate. When the coil is driven by the pulse current, it produces a varying electromagnetic field in the surrounding space. The pulse current is also induced in the aluminum plate near the coils due to the eddy current effect. Since the permanent magnets above the aluminum plate provide a magnetic field perpendicular to the plate surface, a periodic force is generated on the aluminum plate under the effect of the Lorentz force. Due to the periodic

effect of the force, the SH waves generate in the aluminum plate eventually and propagate in opposite directions.

The excitation process of the SH wave involves the coupling between two physical fields: electromagnetic field and dynamic elastic field. The electromagnetic field model mainly calculates the distribution of the eddy currents in the aluminum plate. The Maxwell equations can be utilized to describe the physical process. Fig.1 shows a schematic diagram of the downhole annular two-electrode flow electromagnetic measurement system and the flowpath. A and B represent two electrodes placed on the outside wall at intervals of 180° inside the annular flowpath, N and S represent two magnetic coils inlaid on the wall of the annular flowpath at intervals of 180°, a and b are the distances of the inner and outer surfaces to the center, and ∑1 and ∑2 represent the inner and outer surfaces of the annular flowpath.

$$\sigma \frac{\partial \mathbf{A}}{\partial t} - \frac{1}{\mu} \nabla^2 \mathbf{A} = \mathbf{J}_s, \tag{1}$$

where A is the magnetic field potential; σ is the conductivity; Js is the source current density. The eddy current can be expressed as

$$\mathbf{J}_e = -\sigma \frac{\partial \mathbf{A}}{\partial t}, \tag{2}$$

According to the generation mechanism of Lorentz force, the eddy current distribution calculated by the above formula generates periodic force under the effect of the external static magnetic field and dynamic magnetic field.

$$\mathbf{F}_v = \mathbf{J}_e \times (\mathbf{B}_d + \mathbf{B}_s), \tag{3}$$

Lorentz force plays an important role as a coupling variable that connects the two models. As for the second model, the elastic dynamic model can be expressed in a different form as a wave equation.

$$(\lambda + \mu) \nabla \nabla \cdot \mathbf{u} + \mu \nabla^2 \mathbf{u} + \mathbf{F}_v = \rho \frac{\partial^2 \mathbf{u}}{\partial t^2}, \tag{4}$$

where u is the displacement vector; t is the time; ρ is the mass density; λ and μ are the Lame's constants of the material, which affects the propagation velocity of the shear and longitudinal waves in an aluminum plate.

C. Numerical Algorithm

The calculation of the model was implemented by using the COMSOL software. When calculating the EMAT based on Lorentz force, skin effect and proximity effect need to be considered. The calculation of static magnetic fields and mechanical fields can be done with the built-in modes of COMSOL Multiphysics. The finite element method was utilized in the calculation as meshing is of great significance in the finite element simulation as it affects the calculation efficiency, accuracy, convergence and the identifiability of the results. Therefore, in order to ensure the calculation accuracy, the mesh size should be small enough to ensure the computational feasibility, and the grid quality should be modifiedas high as possible. The skin depth below the surface of the aluminum plate should be set to two or more cells, and it should be ensured that there should be more than seven cell in the wavelength of the ultrasonic waves excited inside the aluminum plate. In this paper, the meshing of the calculation area is shown in Fig. 2, and the grid parameters are shown in Table I.

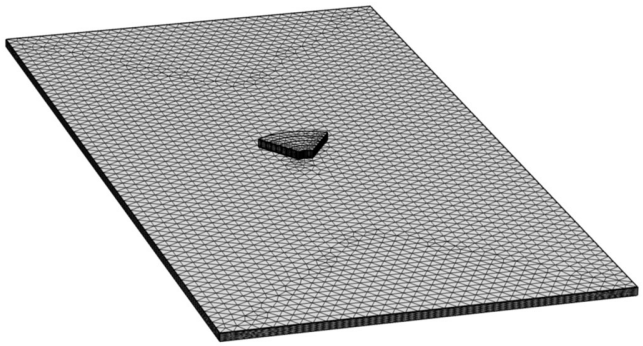

Fig. 2 Computational domain of the simulation (the air domain is omitted).

TABLE I
UNIT DIMENSION PARAMETER OF MESH GENERATION

Parameters	Value
Mesh vertices	457 447
Tetrahedron	2 263 159
Triangle	102 439
Edge element	1 396
Vertex element	18
Number of elements	2 263 159
Minimum unit quality	0.387
Average unit quality	0.993
Unit volume ratio	1.188×10^{-4}
Mesh volume (mm^3)	2.2×10^5

In the process of model solving, the static bias magnetic field is solved in a steady state, and other fields are solved by the transient method. In order to reduce the numerical oscillation of the solution and improve the smoothness and stability of the calculation, the time step (1 ns), relative tolerance (1×10−4), and absolute tolerance (1×10−6) need to be set properly.

The size of the aluminum plate used in the simulation is 200×100×1 mm^3, in order to avoid the interference of the reflected SH waves on the upper and lower surfaces of the aluminum plate, the length of the aluminum plate in the y direction is set to 100 mm. In order to achieve coupling space, air domain is added to the model with a size of 200×100×10 mm^3. For periodic permanent magnets, the intervals D between the adjacent magnets are set to 1.6 mm along the radius direction. It can be explained by the fact that the phase superposition of the SH waves can only be achieved if the distance between the radiant points of the SH waves is equal to a half wavelength.

$$D_i = c_s / 2f, \quad (5)$$

where shear wave velocity c_s =3.2 km/s and f =1 MHz in the paper.

TABLE II
PARAMETERS OF THE SH WAVE EMAT

Parameters	Value
Aperture angle (°)	30
Focal radius (mm)	30
Lift-off distance (mm)	1
Lame's constants λ (GPa)	58
Lame's constants μ (GPa)	29
Aluminum specimen mass density (kg/m^3)	2832
Aluminum specimen conductivity (S/m)	3.65 x 10^7
Remanent magnetism of the magnet (T)	1.2
Relative permeability of the magnet	400

Some physical quantities will change during the analysis. If there is no special explanation, the parameters could be set in Table II.

The dispersion relationship of the SH guided wave can be obtained by analyzing the relationship between the phase velocity c_p and the shear wave velocity c_s.

$$c_p(fd) = 2c_s \frac{fd}{\sqrt{-(nc_s)^2 + 4(fd)^2}}, \quad (6)$$

where f is the drive frequency, d is the thickness of the plate. The phase velocity of the SH0 mode wave does not change with the frequency-thickness product, and the SH0 wave mode has no dispersion. In order to utilize the characteristics of the SH0 mode guided wave, the following formula needs to be satisfied.

$$fd \le \frac{nc_s}{2}, \quad (7)$$

In this paper, n should be greater than 0 to avoid the presence of any higher order wave modes. Then the cutoff frequency of the SH1 mode guided wave is 1.6 MHz. Therefore, in order to generate a pure SH0 mode guided wave, the drive frequency of the AC coil is selected as 1 MHz in the simulation and experiment.

The excitation current is a burst wave with an amplitude of 2 A. The expression of the excitation burst current for the EMAT coils is

$$i(t) = \beta e^{-\alpha(t-\tau)^2} \cos[2\pi f_c(t-\tau) + \theta], \quad (8)$$

where β is the amplitude of the signal, α is the bandwidth factor, τ is the arrival time, f_c is the central frequency, and θ is the phase delay. The value of the parameters above is shown in Table III, and the waveform of the excitation current is shown in Fig. 3.

TABLE III
PARAMETERS OF BURST SIGNALS FOR THE COILS

Parameters	Value
β (A)	2
α	5 x10^{11}
τ (μs)	4
fe (MHz)	1
Θ (°)	0

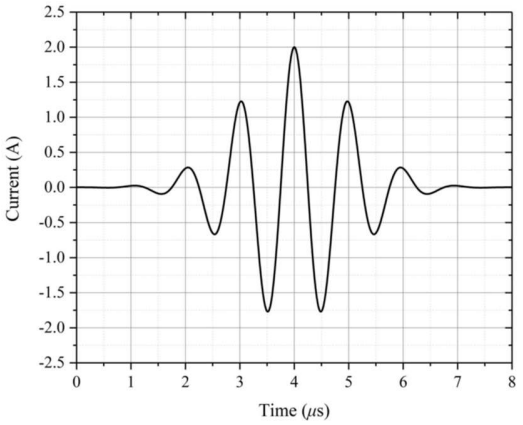

Fig. 3 The waveform of the excitation current.

III. RESULTS

A. Parallel PPA Parellel Coils Emat

To compare and analyze the signal intensity of the two EMATs with parallel PPM parallel coils (PPPC) and fan-shaped PPM focusing coils (FPFC), a simple traditional parallel coil EMAT will be simulated in this paper. Fig. 4 shows a three-dimensional model by using the electromagnetic field mode of the COMSOL Multiphysics software and the solid mechanic's mode with the linear elastic material.

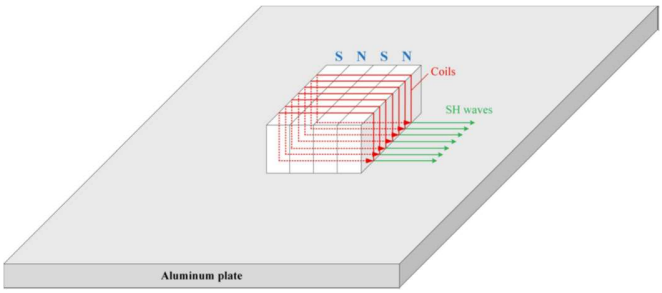

Fig. 4 Configuration setup for the PPPC EMAT

In the simulation, the spacings of the adjacent coils are set to 5 mm. The current magnitude and the phase of the seven coils are consistent. The spacings between the periodic permanent magnets are maintained at a half wavelength, i.e., 1.6 mm. For the waves propagating along the surface of the aluminum plate, the SH guided waves generated by the adjacent coils will superimpose and interfere at different positions of the plate. It is mentioned above that the propagation velocity of the transverse wave in the plate is 3.2 km/s, and the effective propagation distance along one side of the plate is 100 mm. Therefore, it is known from the calculation that the SH wave

will reach the boundary of the plate at about 30 μs. Since the paper mainly focuses on the amplitude variation of the signal along the direction of the guided wave, the unilateral width of the plate is set to 50 mm in order to improve the simulation efficiency. The shear wave reflection generated on both sides of the plate will affect the signal amplitude. Therefore, the calculation time should be less than 19 μs in the simulation considering excitation delay of the burst signal. In this paper, four typical moments of 10 μs, 13 μs, 16 μs, and 19 μs are selected for the displacement analysis of the plate surface. It is shown in Fig. 5(a–d) that the distributions of the displacement field at four different moments demonstrate the traveling characteristics of the SH waves.

As shown in the figures, it can be shown that the SH guided waves propagate bidirectionally along the x-axis and the amplitude decays as the time increases. The SH guided waves generated by the seven coils are superimposed on each other on the surface of the aluminum plate, and the ultrasonic energy is gradually concentrated to the x-axis where the center coil is located. Moreover, because of the symmetrical placement of the coil structure, it can be found that the displacement field distribution on both sides of the transducer is highly uniform so that energy leakage is easily generated when detecting defects in a specific direction on the aluminum plate.

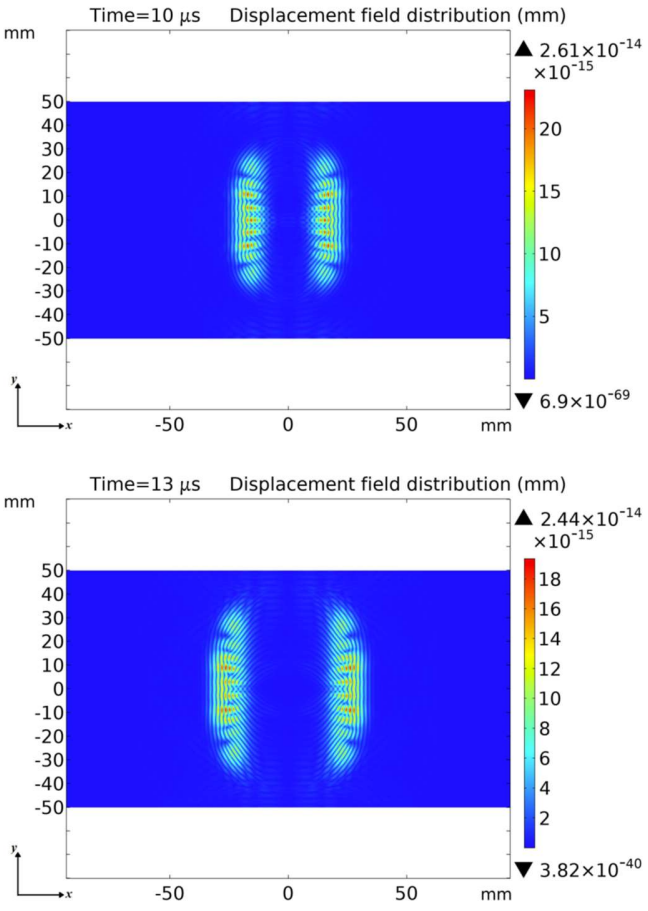

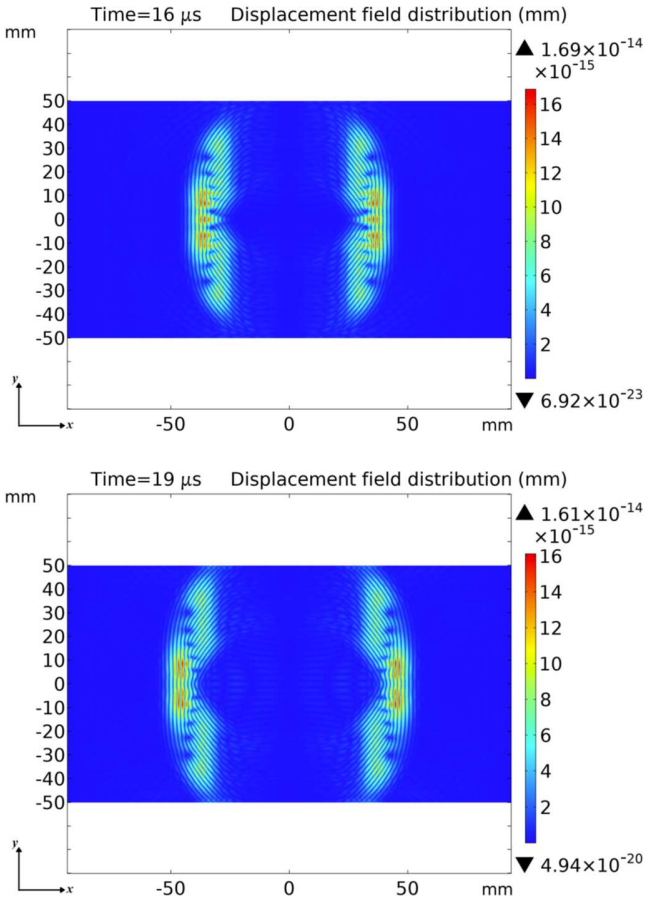

Fig. 5 Simulation results for the PPPC EMAT. Including the distribution of the displacement field on the aluminum plate at: (a) 10 μs, (b) 13 μs, (c) 16 μs, and (d) 19 μs.

B. Fan-Shaped PPM Focusing Coils Emat

By analyzing the simulation results of the previous section, it can be found that the traditional PPPC EMAT is suitable for the detection of the aluminum plate. However, the bidirectional propagation characteristics of the SH guided wave cause the weakened signal intensity and signal-to-noise ratio. Therefore, the detection of the focusing in a certain direction or a certain point of the aluminum plate is of great significance.

The excitation direction of the SH guided wave based on the Lorentz force mechanism is generally consistent with the direction of the coil, and adjusting the spacings of the periodic permanent magnets will change the phase of the focal position.

Therefore, it can be assumed that adjusting the direction of the coil will change the propagation direction of the SH guided wave, and adjusting the spacings of the periodic permanent magnets will change the superposition effect of the wave phase. The principle of the half-wavelength superposition of the SH waves is introduced in the previous section, then the spacings of periodic permanent magnets in this paper are set to 1.6 mm ($\lambda/2$). However, since the focusing coils are not parallel, the parallel periodic permanent magnets are not suitable for the half-wavelength requirement, so a method of fan-shaped permanent magnets is proposed to ensure the superposition of

phases.

Seven coils with an aperture angle of 60◦ are utilized in the simulation with a focal radius of 30 mm and a sector-shaped permanent magnet with an aperture angle of 90◦. In order to compare with the PPPC EMAT in the previous section, the simulation time is also set to 20 μs, and the distributions of the displacement field of 10 μs, 13 μs, 16 μs, and 19 μs are extracted for comparison in Fig. 6(a)–(d). For quantitative analysis, the displacement field distribution along the x-axis on the surface of the aluminum plate is shown in Fig. 7(a), (b) at 13 μs, which is the focusing moment of the FPFC EMAT. It can be seen from the figure that the SH-guided EMAT using the focusing structure can unidirectionally converge the signal while generating the dispersion of the signal on the other side. As can be shown from the figures, the signal intensity at the focal point position is significantly improved, and the signal amplitude on the other side is reduced. Table IV shows the calculation results of the FPFC EMAT and the boost ratio of this configuration.

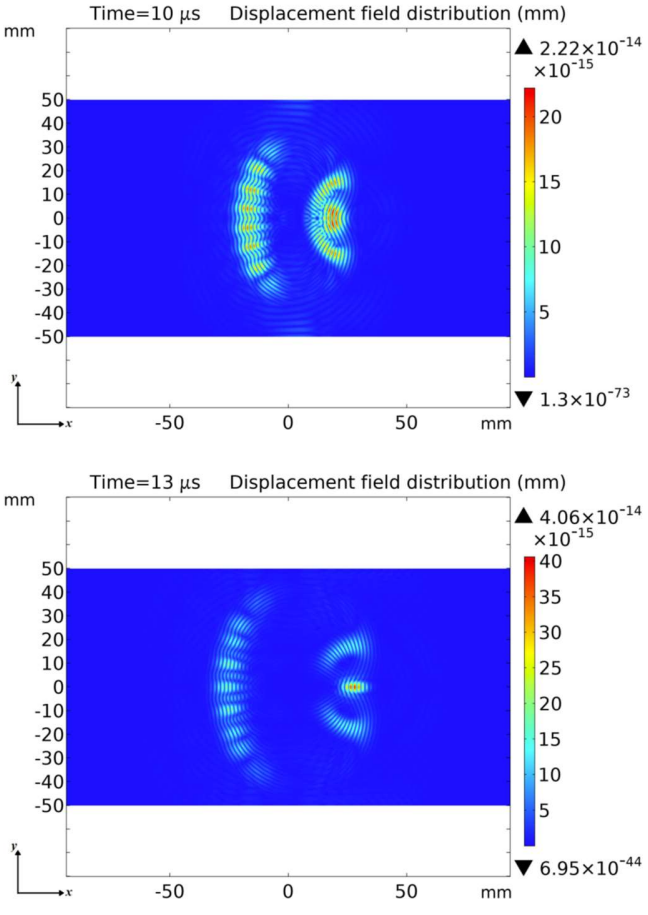

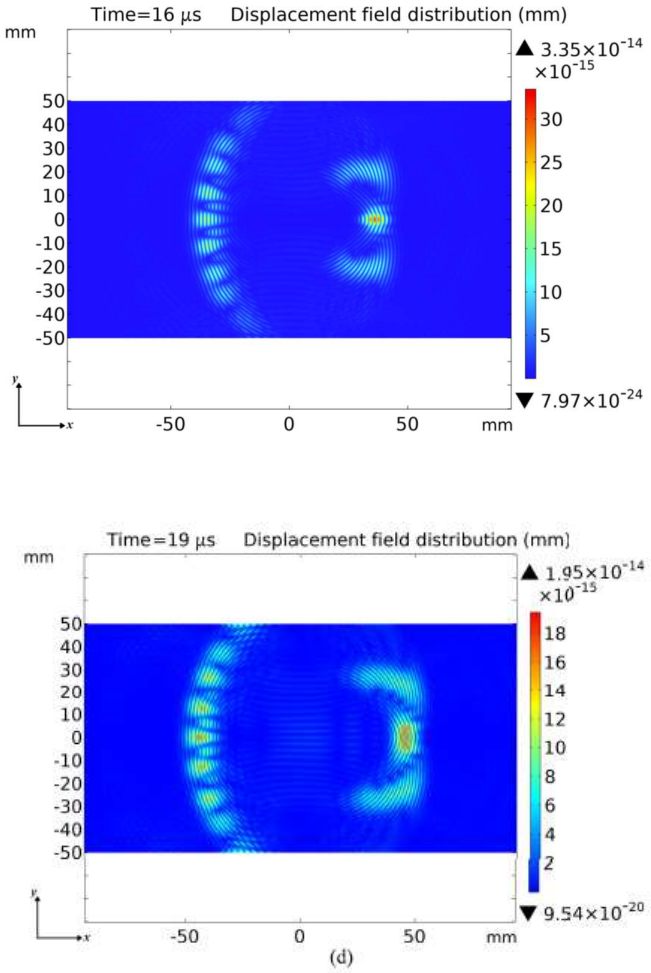

Fig. 6. Simulation results for the FPFC EMAT. Including the distribution of the displacement field on the aluminum plate at: (a) 10 μs, (b) 13 μs, (c) 16 μs, and (d) 19 μs.

The amplitude of the signal on the focus side is 92.86 higher than the amplitude of the signal on the diverging side at the focal point and its symmetrical position, which proves that most of the guided wave energy is indeed focused at a predetermined point. It can be found that the average distance between the focus coils is 5 mm, so the comparative analysis can be performed by setting the spacings of the parallel coils to 5 mm. The simulation results show that the amplitude of the signal intensity at the same position (focal point) between PPPC EMAT and FPFC EMAT is very different at the same time. The focusing coils generate the displacement at the focal point where the boost ratio is 68.75% higher than the displacement produced by the parallel coil. This demonstrates that the new focusing transducer structure can greatly increase the amplitude of the signal at the focal position.

TABLE IV
THE MAGNITUDE OF THE DISPLACEMENT FIELD AT THE FOCAL POINT AND THE BOOST RATIO

Focusing side (mm)	Divergent side (mm)	Difference between two sides	Boost ratio to parallel coils
4.05 x 10^{-14}	2.1 x 10^{-14}	92.86%	68.75%

C. *Defect detection by PPPC & the FPFC EMATs*

The focusing capability of the FPFC EMAT is discussed above with the PPPC EMAT, so it is then necessary to study the defect detection capability for the two EMATs.

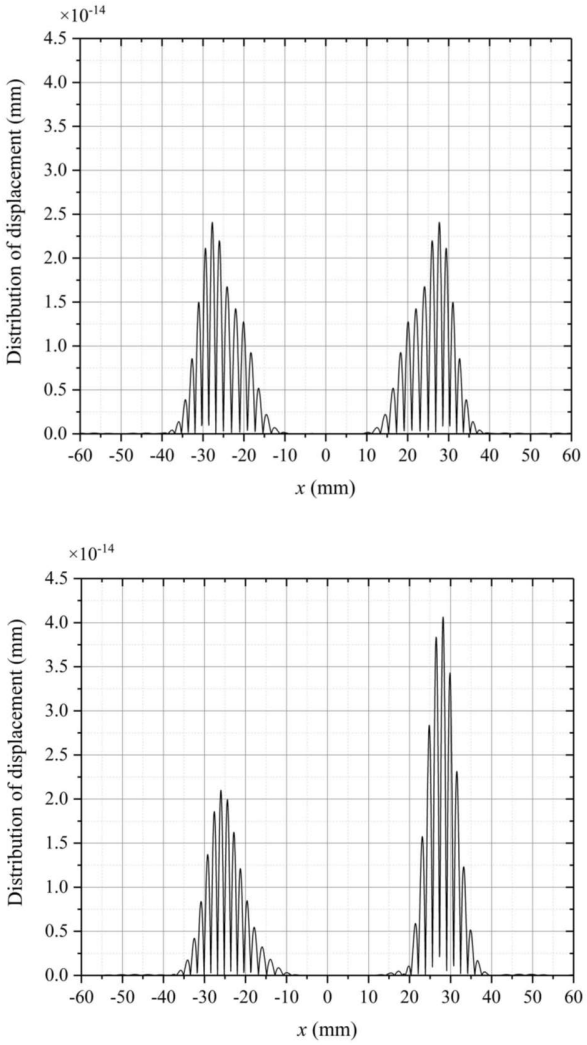

Fig. 7. The displacement distribution along the x-axis on the aluminum plate at 13 μs. (a) PPPC EMAT, (b) FPFC EMAT.

The artificial cuboid defect with a size of 1×3×0.5 mm3 is set at the focal point of the new EMAT, as well as the same defect position for the traditional EMAT. The moment (14.5 μs) is selected shortly after the SH guided waves encounter the artificial defect to calculate the simulation result, and the displacement field distributions of the two EMATs are shown in Fig. 8(a), (b).

It can be seen from the figure that the SH guided wave will refract and reflect when it encounters a defect, and the reflected wave intensity of the FPFC EMAT is significantly higher than that of the PPPC EMAT. To study the detection capabilities of different transducers in the presence of defects in detail, the position (10 mm, 0 mm) on the plate surface is selected in Fig. 9(a), (b) to show the displacement variation of this point as the time increases. The first pulse in the figure is generated by the SH guided waves, while the second one is generated by the reflected waves. It can be obtained from Fig. 9(a) that the reflected signal is weaker than the first one, which can be explained by the reason that the intensity of ultrasound will be weakened with the increase of the propagation distance and the reflection. However, for the signal of the new FPFCm EMAT in Fig. 9(b), the reflected signal is shown has the same amplitude as the initial signal. Moreover, the reflected signal intensity of the FPFC EMAT is much higher (nearly two times) than that of the PPPC EMAT, which proves the high focusing capability of the new EMAT.

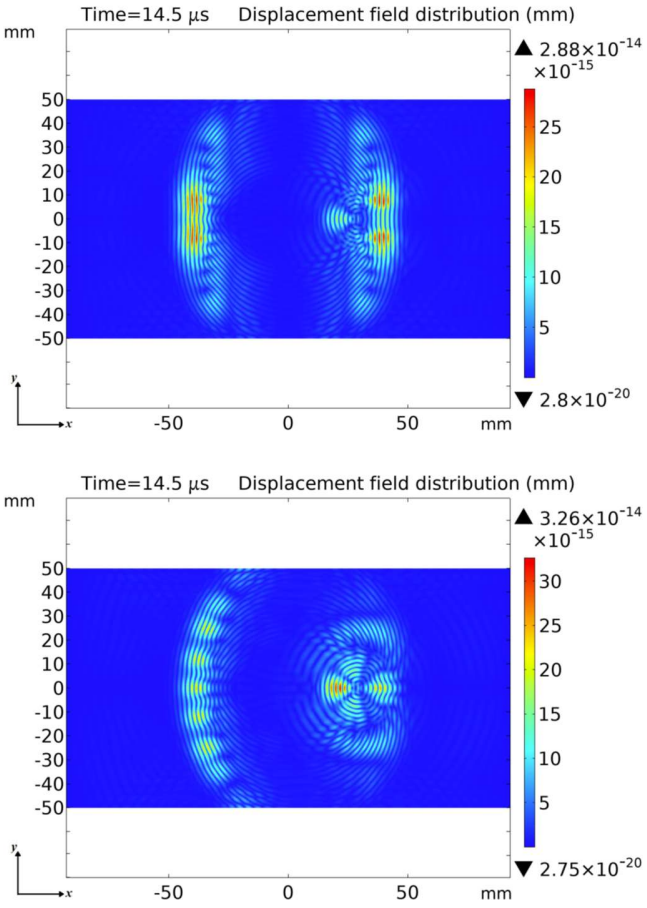

Fig. 8. Displacement field distribution with artificial defects at 14.5 μs. (a) PPPC EMAT. (b) FPFC EMAT.

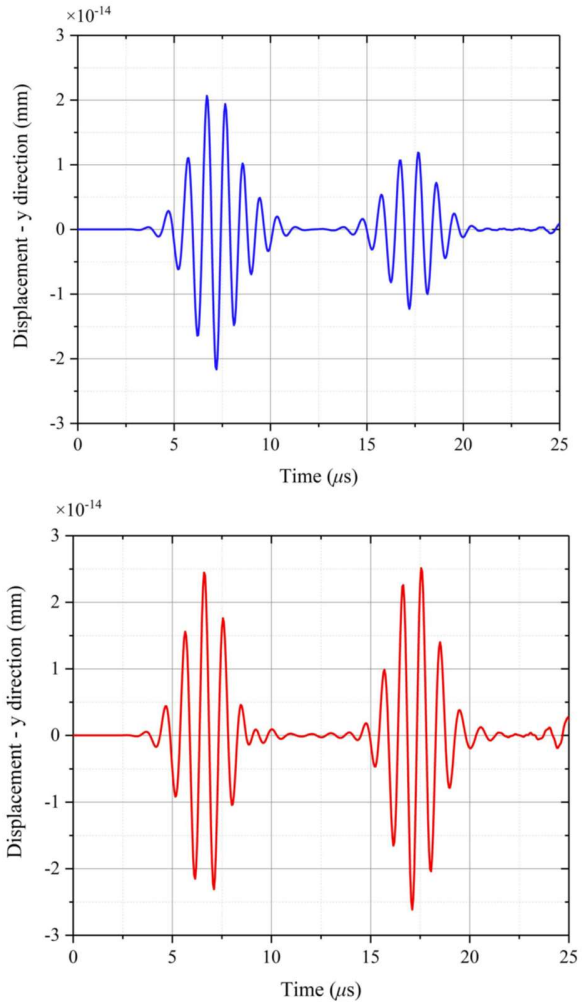

Fig. 9. The displacement variation along y-direction at (10 mm, 0 mm) on the plate surface. (a) PPPC EMAT. (b) FPFC EMAT.

IV. DISCUSSIONS

As the propagation distance increases, the amplitude of the SH wave is attenuated, and the propagation direction also has a specific attenuation. Therefore, the design of the coil structure of the focusing transducer is very significant. Due to the phase superposition effect of the half wavelength, the pitch of the periodic permanent magnet has been determined to 1.6 mm as discussed above. Therefore, the influence of the focal radius and the aperture angle on the focusing effect also needs to be studied while the other parameters remain unchanged. As the increase in coil winding number and the increase in the excitation current will inevitably lead to an increase in the displacement of the focal point, both of the above factors will be fixed in the simulation and experiment to ensure the comparability of the results. Fig. 10 shows the FPFC EMAT with five different aperture angles and four focal radii. It can be seen from the figure that as the aperture angle of the coil increases, the amplitude of the normalized signal of the focus point decreases linearly. Furthermore, the larger the aperture angle is, the lower the waveform superposition effect at the focus point is while the number of turns of the coil is fixed. Since the surface of the aluminum plate can be regarded as an approximate two-dimensional vibration field, under the influence of two vibration sources with the same phase and the same amplitude but at different positions, the main influencing factor of the superposition effect is the polarization direction of the SH wave. An increase in the angle of polarization of the two causes a decrease in signal intensity.

It can be seen from the figure that as the focal radius increases, the slope of the linear relationship of the normalized amplitude-aperture angle magnitude will decrease. Therefore, an increase in the focus radius leads to a significant decrease in the effect of the aperture angle. When the length of the focus radius is relatively small, the effect of the aperture angle on the normalized amplitude is more significant. Since the increase in the focus radius causes the attenuation of the signal amplitude, the distance of the focus point will cause an approximately exponential decay of the normalized amplitude under the same aperture angle. Therefore, from the results and analysis above, it is known that in the design process of the FPFC EMAT, the focus radius and the aperture angle should not be large. When the number of the coil windings can be changed, a larger aperture angle will certainly bring more coils and higher signal intensity, so it is necessary to focus on the focal radius during the design process of the new EMATs.

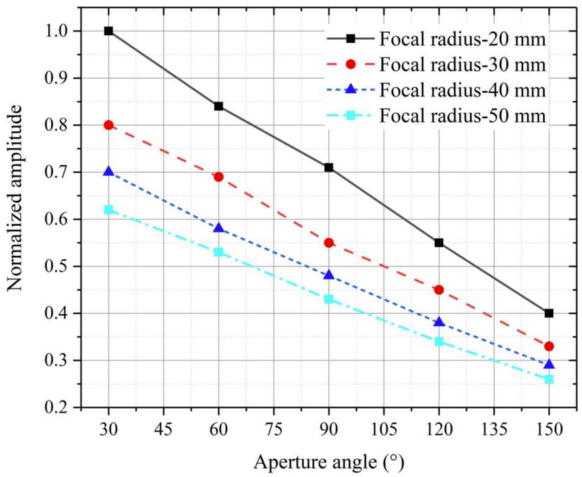

Fig. 10. The influence of the aperture angles and the focal radii on the normalized amplitude of the displacement field.

To study the effect of the focal radius on the focusing capability of the new FPFC EMAT, four focal radii 20 mm, 30 mm, 40 mm and 50 mm are selected in the simulation. In the selection of the simulation time, the time when the peak value of the SH guided wave reaches the focal point is equivalent to the time summation: the shear wave propagation and the excitation delay of the burst signal. Therefore, the focusing moments of the different focal radii are 10.35 μs, 13.55 μs, 16.75 μs, and 19.95 μs. The displacement field distributions under the above conditions are shown in Fig. 11(a)–(d). It can be seen from the figures that the SH guided waves always focus on the focal point regardless of the focal radius, and the amplitude of the displacement on the focusing side is much larger than that on the divergent side. To study the focusing capability of the transducers with different focal radii, Fig. 12 shows the y-direction displacement distribution along the x-axis

at different focal radii and focusing moments. Moreover, the differences between the focusing side and the divergent side at different focal radii are shown in Fig. 13, as well as the maximum y-direction displacements at these moments. These figures show that as the focal radii increase, although the amplitude of the signal on the focusing side decreases, the amplitude of the signal on the divergent side decreases faster. Also, in the range of the simulated focal radius, the difference between the two sides increases exponentially as the focal radius increases, and the weak divergent side signal will improve the signal-to-noise ratio of the signal received by the receiving transducer. Therefore, a reasonable selection of the focal radius is important for achieving higher signal intensity and signal-to-noise ratio simultaneously.

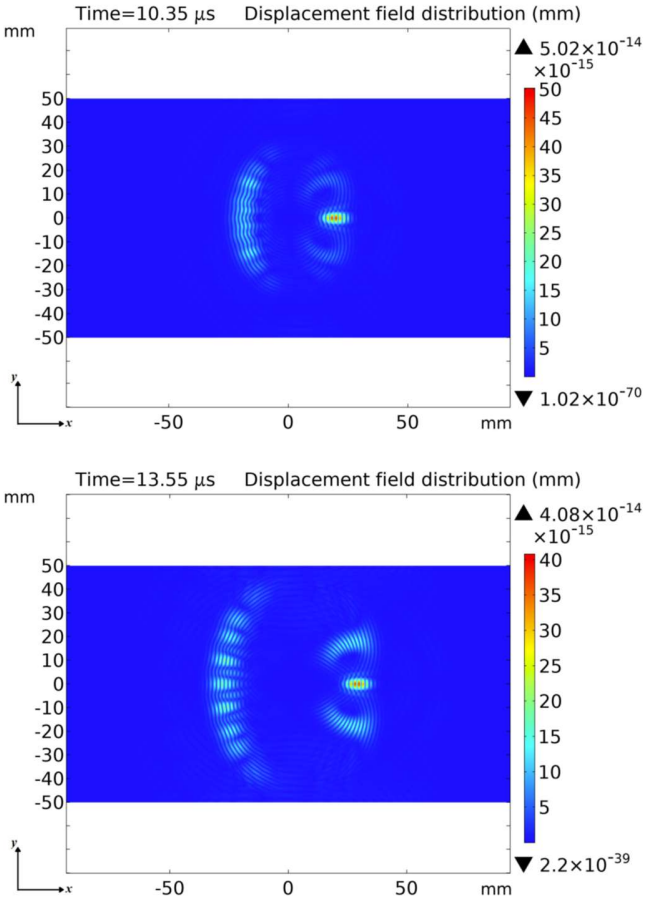

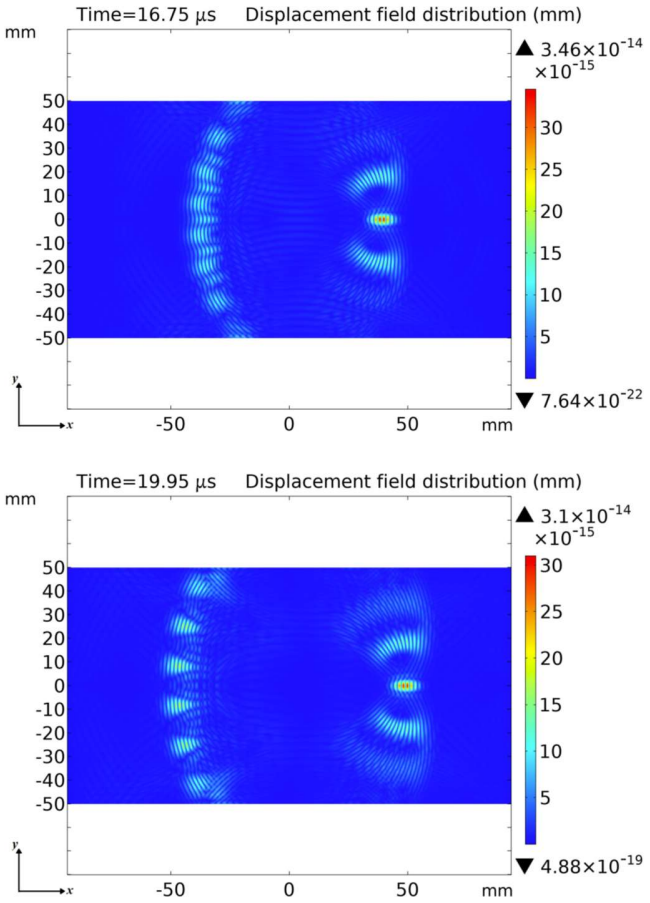

Fig. 11. Displacement field distribution. (a) Focal radius is 20 mm at 10.35 μs. (b) Focal radius is 30 mm at 13.55 μs. (c) Focal radius is 40 mm at 16.75 μs. (a) Focal radius is 50 mm at 19.95 μs.

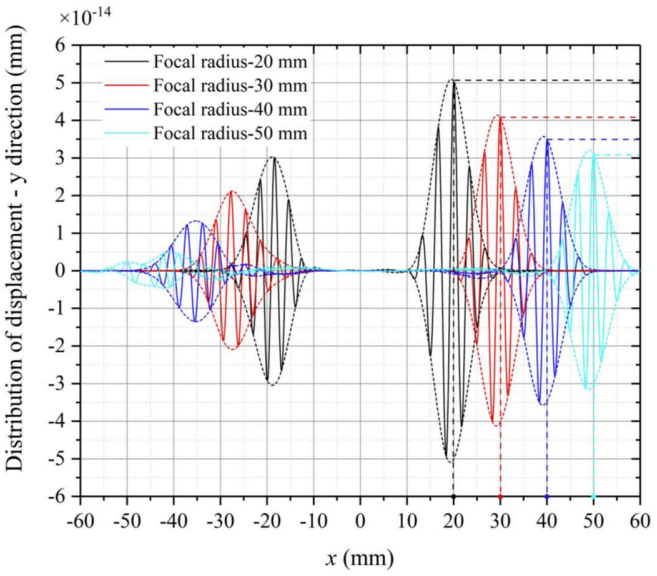

Fig. 12. y-direction displacement distribution along x-axis at different focal radii and focusing moments.

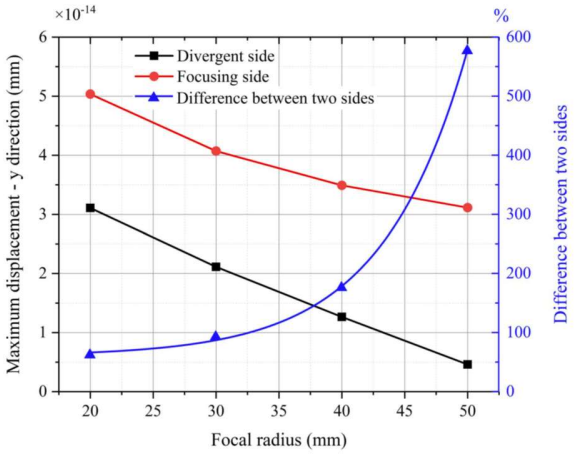

Fig. 13. The maximum y-direction displacements, and the differences between the focusing side and the divergent side at different focal radii.

The new focusing EMAT is developed and discussed above using finite element simulation method. An experiment platform corresponding to the simulation conditions has been built and the configuration of the experimental setup is shown in Fig. 14. The material of the specimen is aluminum, and the size is 200×100×1 mm3 in the experiment. The coils are excited by a burst current with an amplitude of 2 A and bandwidth factor of 5×1011, which can be controlled by the RPR-4000 power and the programming method. Pulsed power (RPR 4000) for generating and receiving signals are utilized in the experimental research. The power not only produces strong and stable sinusoidal high-frequency pulses but also identifies and receives the desired signals over a broad frequency band. The oscilloscope (TDS 1002) is utilized to display the waveform acquired by the RPR-4000 with the bandwidth of 60 MHz and the sampling rate of 1 Gs/s.

The structures of the transmitter and the receiver are the same, and the experimental conditions are consistent with the simulation conditions. Moreover, the focal positions of the transmitter and receiver are identical when measuring the signal intensity at the focal point. As for the defect detection, the arrangement of the transmitter and the receiver are placed at a certain position, which is shown in Fig. 14. The receiver is 20 mm away from the transmitter. The measured signals of traditional PPPC EMAT and new FPFC EMAT are shown in Fig. 15(a), (b), and the signals based on the FEM models are also shown in Fig. 15. Due to the low energy conversion efficiency of EMAT, high-power pulse current excitation is required. Therefore, in order to obtain the maximum output power of the excitation source, it is required to match the impedance of the load with the internal impedance of the excitation source, then 150 ohms matching impedance are utilized in the experiment to improve the accuracy and the efficiency of the EMAT. EMATs for receiving and transmitting signals are new-designed FPFC EMATs. The EMAT's focal positions (focal radii) are set to different values under the same conditions, and the experimental results are compared with the simulation results (Fig. 16).

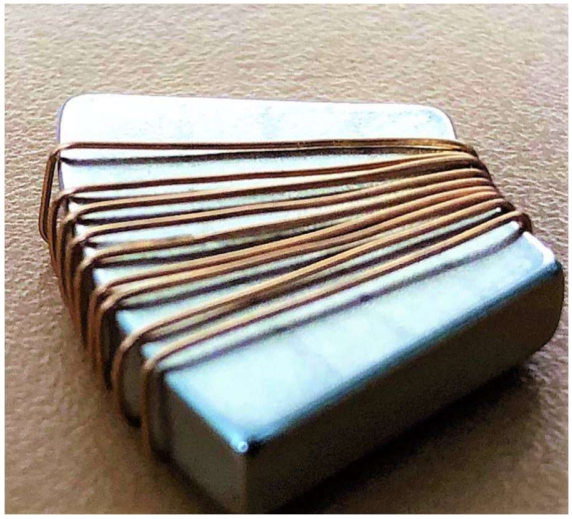

(a)

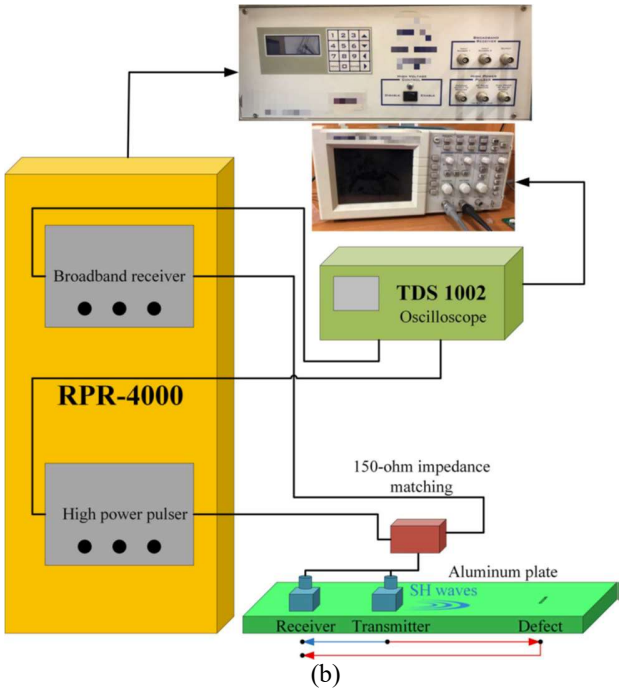

(b)

Fig. 14. The maximum y-direction displacements, and the differences between the focusing side and the divergent side at different focal radii.

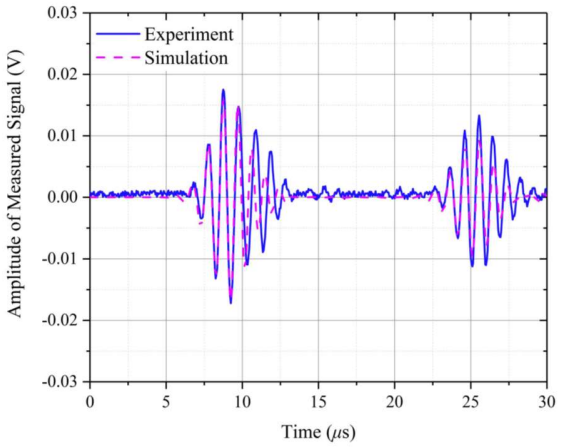

Fig. 15. Measured signals from simulation and experiment. (a) Traditional PPPC EMAT. (b) New FPFC EMAT.

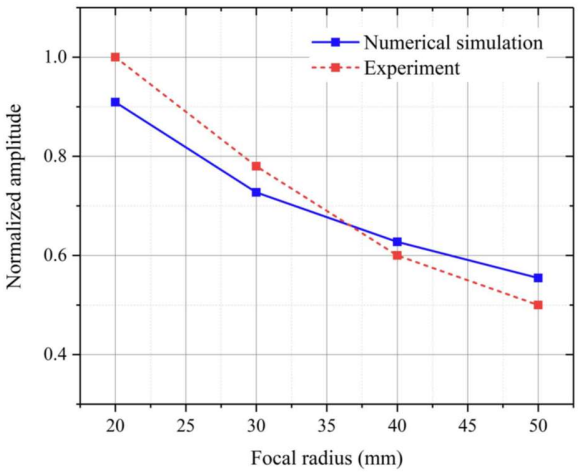

Fig. 16. Normalized amplitude of signal intensity at different focal radii with simulation and experimental verification.

It can be seen from the figure that the simulation results are in good agreement with the experimental results. In order to avoid the interference of the reflected wave on the signal during the simulation, the total simulation time is set at the moment (20 μs) when the SH wave just reaches the boundary position. In the experiment, the influence of the reflected wave cannot be ignored, so the results between the simulation and experiment are shown with a small difference. According to the experimental results, similar conclusions can be obtained and it is proved that an increase in the focal radius results in a decrease in the signal intensity at the focal point position. In the practical application of the focusing transducer, the accuracy error caused by the manufacturing process may lead to the asymmetry of the coil winding. The problem with the EMAT proposed in this paper is embodied by the eccentricity and rotation of the radial concentric coils. The asymmetry of the typical coils is mainly reflected in the direction deviation of a certain coil of the EMAT. Therefore, it is necessary to study the rotation angle of a coil in the focusing transducer.

In this paper, the rotation angle of the coil is defined as: The center of the coil is the rotation center, and the angle formed by the radial direction deviating from the focal point is the direction of rotation. Fig. 17 shows the definition of the rotation angle ϕ and the setting of the simulation geometry model, the seven-coil structure is also utilized in the simulation while the upper coil has a rotation angle.

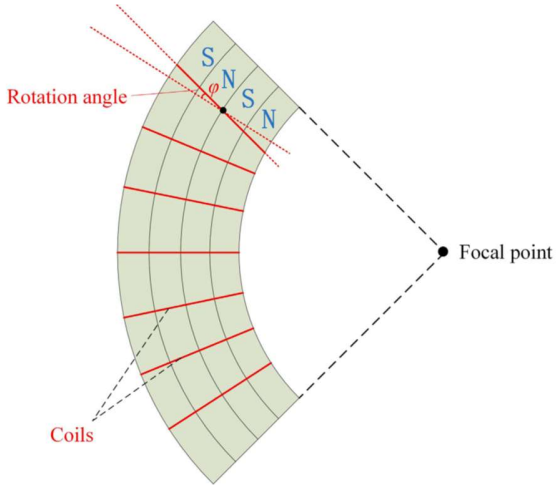

Fig. 17. The definition of the rotation angle ϕ and the setting of the simulation geometry model.

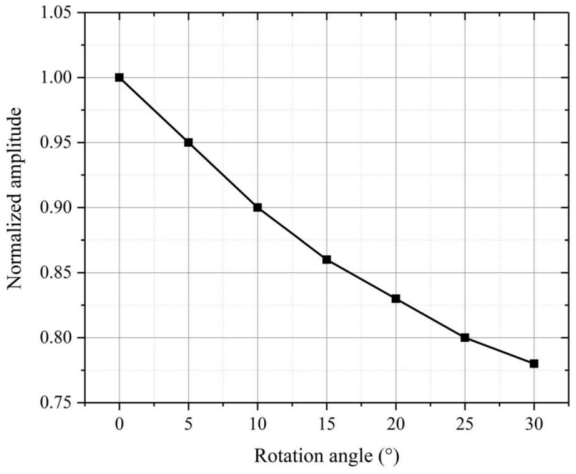

Fig. 18. The effect of different rotation angles of a single coil on the normalized displacement amplitude of the focal point through simulation.

Fig. 18 shows the effect of different rotation angles of a single coil on the normalized amplitude of the displacement of the focal point position through simulation. It can be seen from the figure that as the rotation angle ϕ of the coil increases, the normalized displacement amplitude of the focal point decreases parabolically. If $\phi \geqslant 30^{\circ}$, the contribution of the rotating coil to the signal focusing intensity of the entire transducer can be neglected. When the rotation angle of the coil reaches about 10°, the contribution of the coil to the focusing ability has been halved. Therefore, the rotation of the coils will greatly affect the focusing characteristics of the new-designed focusing EMAT, even with only a few degrees of the angular difference.

V. Conclusions

A new-designed fan-shaped PPM focusing coils EMAT has been carried out to focus the SH waves at a certain point utilizing a numerical simulation method with experimental validation. The reflected signal intensity of the FPFC EMAT is much higher (nearly two times) than that of the traditional PPPC EMAT. Therefore, the new-designed FPFC EMAT have a great advantage in defect detection. The results show that the signal intensity on the focusing side of the focusing EMAT is 92.86% higher than that on the divergent side. Moreover, the signal intensity at the focal point of the traditional EMAT is increased by 68.75%, which proves that most of the guided wave energy is indeed focused at a certain point.

As for the other factors, the influence of the aperture angle and focal radius on the EMAT focusing ability are also investigated in the study. According to the simulation calculation and the experimental verification, the conclusions can be drawn as follows. As the aperture angle of the coil increases, the amplitude of the normalized ultrasonic signal of the focal point decreases linearly. Furthermore, as the focal radius increases, although the amplitude of the signal on the focusing side decreases, the amplitude of the signal on the divergent side decreases faster. Also, the difference between the two sides increases exponentially as radius increases, and the slope of the linear relationship of the "normalized amplitude - aperture angle magnitude" will decrease. The asymmetrical rotation angle of the coil is also studied in this paper that the normalized displacement amplitude of the focal decreases parabolically as the rotation angle ϕ of the coil increases.

VI. Acknowledgments

The authors would like to thank Dr. Lisha Peng (pls14@mails.tsinghua.edu.cn) for English writing assistance in the paper.

References

[1] X. Jia and Q. Ouyang, "Optimal design of point-focusing shear vertical wave electromagnetic ultrasonic transducers based on orthogonal test method," IEEE Sensors J., vol. 18, no. 19, pp. 8064–8073, Oct. 2018.

[2] R. Ribichini, F. Cegla, P. B. Nagy, and P. Cawley, "Experimental and numerical evaluation of electromagnetic acoustic transducer performance on steel materials," NDT & E Int., vol. 45, no. 1, pp. 32–38, 2012.

[3] S. Legendre, D. Massicotte, J. Goyette, and T. K. Bose, "Neural classification of Lamb wave ultrasonic weld testing signals using wavelet coefficients," IEEE Trans. Instrum. Meas., vol. 50, no. 3, pp. 672–678, Jun. 2001.

[4] S. Legendre, D. Massicotte, J. Goyette, and T. K. Bose, "Wavelet transform-based method of analysis for Lamb-wave ultrasonic NDE signals," IEEE Trans. Instrum. Meas., vol. 49, no. 3, pp. 524–530, Jun. 2000.

[5] H. Ogi, M. Hirao, and T. Ohtani, "Line-focusing of ultrasonic SV wave by electromagnetic acoustic transducer," J. Acoust. Soc. Amer., vol. 103, no. 5, pp. 2411–2415, 1998.

[6] H. Ogi, M. Hirao, and T. Ohtani, "Line-focusing electromagnetic acoustic transducers for the detection of slit defects," IEEE Trans. Ultrason., Ferroelectr., Freq. Control, vol. 46, no. 2, pp. 341–346, Mar. 1999.

[7] P. A. Petcher and S. Dixon, "Weld defect detection using PPM EMAT generated shear horizontal ultrasound," NDT & E Int., vol. 74, pp. 58–65, Sep. 2015.

[8] J. S. da Rocha Neto, "Development of circuits for excitation and reception in ultrasonic transducers for generation of guided waves in hollow cylinders for fouling detection," IEEE Trans. Instrum. Meas., vol. 57, no. 6, pp. 1149–1153, Jun. 2008.

[9] S. S. Lee and B. Y. Ahn, "EMAT application at high temperature,"
Nondestruct. Test. Eval., vol. 7, nos. 1–6, pp. 253–261, 1992.

[10] P. S. Lowe, R. M. Sanderson, N. V. Boulgouris, A. G. Haig, and W. Balachandran, "Inspection of cylindrical structures using the first longitudinal guided wave mode in isolation for higher flaw sensitivity," IEEE Sensors J., vol. 16, no. 3, pp. 706–714, Feb. 2016.

[11] E. Glushkov, N. Glushkova, A. Eremin, and R. Lammering, "Group velocity of cylindrical guided waves in anisotropic laminate composites," J. Acoust. Soc. Amer., vol. 135, no. 1, pp. 148–154, 2014.

[12] S. M. Keller, A. E. Sepulveda, and G. P. Carman, "Effective magnetoelectric properties of magnetoelectroelastic (multiferroic) materials and effects on plane wave dynamics," Prog. Electromagn. Res., vol. 154, pp. 115–126, Dec. 2015.

[13] W. Ren, J. He, S. Dixon, and K. Xu, "Enhancement of EMAT's efficiency by using silicon steel laminations back-plate," Sens. Actuators A, Phys., vol. 274, pp. 189–198, May 2018.

[14] C. Pei, P. Xiao, S. Zhao, and Z. Chen, "Development of a flexible film electromagnetic acoustic transducer for nondestructive testing," Sens. Actuators A, Phys., vol. 258, pp. 68–73, May 2017.

[15] C. Pei, S. Zhao, P. Xiao, and Z. Chen, "A modified meander-line-coil EMAT design for signal amplitude enhancement," Sens. Actuators A, Phys., vol. 247, pp. 539–546, Aug. 2016.

[16] H. M. Seung, C. I. Park, and Y. Y. Kim, “An omnidirectional shear horizontal guided wave EMAT for a metallic plate,” Ultrasonics, vol.pp. 58–66, Jul. 2016.

[17] X. Zhao and J. L. Rose, “Guided circumferential shear horizontal waves in an isotropic hollow cylinder,” J. Acoust. Soc. Amer., vol. 115, no. 5, pp. 1912–1916, 2004.

[18] J. K. Lee, H. W. Kim, and Y. Y. Kim, “Omnidirectional Lamb waves by axisymmetrically-configured magnetostrictive patch transducer,” IEEE Trans. Ultrason., Ferroelectr., Freq. Control, vol. 60, no. 9, pp. 1928–1934, Sep. 2013.

[19] R. Ribichini, F. Cegla, P. B. Nagy, and P. Cawley, “Study and comparison of different EMAT configurations for SH wave inspection,” IEEE Trans. Ultrason., Ferroelectr., Freq. Control, vol. 58, no. 12, pp. 2571–2581, Dec. 2011.

[20] D. Zhang, Z. Zhou, J. Sun, E. Zhang, Y. Yang, and M. Zhao, “A magnetostrictive guided-wave nondestructive testing method with multifrequency excitation pulse signal,” IEEE Trans. Instrum. Meas., vol. 63, no. 12, pp. 3058–3066, Dec. 2014.

[21] S. Hill and S. Dixon, “Frequency dependent directivity of periodic permanent magnet electromagnetic acoustic transducers,” NDT & E Int., vol. 62, pp. 137–143, Mar. 2014.

[22] N. Nakamura, H. Ogi, and M. Hirao, “Detection of shear horizontal guided waves propagating in aluminum plate with thinning region,” Jpn. J. Appl. Phys., vol. 50, no. 7S, 2011, Art. no. 07HC17.

[23] R. B. Thompson, “Physical principles of measurements with EMAT transducers,” Phys. Acoust., vol. 19, pp. 157–200, Nov. 1990.

[24] Y. Zhang, S. Huang, S. Wang, and W. Zhao, “Direction-controllable electromagnetic acoustic transducer for SH waves in steel plate based on magnetostriction,” Prog. Electromagn. Res., vol. 50, pp. 151–160, Sep. 2016.

[25] X. Song and G. Qiu, “Optimization of a focusable and rotatable shearwave periodic permanent magnet electromagnetic acoustic transducers for plates inspection,” Sensors, vol. 17, no. 12, p. 2722, 2017.

Hongyu Sun received a B.S. degree from the Department of Renewable Energy, North China Electric Power University, Beijing, China, in 2015, and a master’s degree from the Department of Electrical and Electronic Engineering, North China Electric Power University, in 2018. He is currently pursuing a Ph.D. degree with the Department of Electrical Engineering, Tsinghua University. His major research interests include electromagnetic measurement, nondestructive evaluation, and plasma physics.

Shen Wang received bachelor’s and Ph.D. degrees in electrical engineering from Tsinghua University, Beijing, China, in 2002 and 2008, Respectively. He is currently a Research Assistant with the Department of Electrical Engineering, Tsinghua University. His research interests include nondestructive testing and evaluation, and virtual instrumentation.

Songling Huang received a bachelor’s degree in automatic control engineering from Southeast University, Nanjing, China, in 1991, and a Ph.D. degree in nuclear application technology from Tsinghua University, Beijing, China, in 2001. He is currently a Professor with the Department of Electrical Engineering, Tsinghua University. His research interests include nondestructive evaluation and instrument techniques.

Qing Wang received the B.Eng. degree in electronic instrument and measurement technique from Beihang University, Beijing, China, in 1995, the M.Sc. degree in advanced manufacturing and materials from the University of Hull, Hull, U.K.,in 1998, and the Ph.D. degree in manufacturing management from De Montfort University, Leicester, U.K., in 2001. She is currently an Associate Professor with the School of Engineering and Computing Sciences, Durham University, Durham, U.K. Her research interests include electronic instruments and measurement, computer simulation, and advanced manufacturing technology.

Wei Zhao received the bachelor’s degree in electrical engineering from Tsinghua University, Beijing, China, in 1982, and the Ph.D. degree from the Moscow Power Engineering Institute Technical University, Moscow, Russia, in 1991. He is currently a Professor with the Departmentmof Electrical Engineering, Tsinghua University. His research interests include modern electromagnetic measurement and instrument techniques.